ADVANCED HEALTHCARE MATERIALS
www.advhealthmat.de

Tattoo Conductive Polymer Nanosheets for Skin-Contact Applications

Alessandra Zucca, Christian Cipriani, Sudha, Sergio Tarantino, Davide Ricci, Virgilio Mattoli, and Francesco Greco**

The increasing demand for portable and ubiquitous electronic applications generated a great interest in the emerging technology area of conformable electronics: a class of materials and electronic devices that are able to adhere and conform to surfaces.[1,2] Advancements in conformable and stretchable electronics are strongly impacting bioinspired and biointegrated technologies. Notable examples are sensorized and smart electronic skin,[1] novel sensing,[3] actuation and energy-harvesting systems[4–6] with applications in consumer electronics, energy, robotics, and biomedicine.[7–9]

As regards the development of human–device interfaces—e.g., smart textiles,[10] wearable electronics,[11,12] and bioelectronics for implantation or unperceivable skin-contact personal health monitoring[13–16]—their design is focused primarily on portability and comfort to achieve a seamless interaction between user and devices.[1,17] In this framework, the term "tattoo electronics" or "epidermal electronics" refers to a variety of conformable electronic devices that can be transferred on the skin.[17]

From a structural point of view, the use of "soft" materials that imitate the mechanical properties of the skin (suitable elastic moduli), associated with the ultralow thickness of structures, allows for an intimate conformal contact with the nonplanar features and surface irregularities of the skin. Different types of materials and design strategies have been adapted to this aim. Inorganic electronic materials were embedded within thin elastomeric substrates in the form of microstructures that are able to withstand stretching.[18–20] Skin-contact applications of this technology include thermal monitoring of the human skin[21] or epidermal hydration sensing.[22,23] On the other hand, organic conductors and semiconductors, which are generally softer than their inorganic counterpart, have also been considered. Flexible, stretchable, and conformable organic field-effect transistors (OFETs), organic light-emitting diodes (OLEDs), connectors, solar cells, and other passive and active organic electronic components have been proposed.[7,12,24–28]

Recently, our group presented ultrathin and ultraconformable nanosheets composed of the conducting polymer complex poly(3,4-ethylenedioxythiophene): poly(styrenesulfonate) (PEDOT:PSS).[29] After their release in water from their temporary substrate, nanosheets can be manipulated as freestanding films, characterized by ultraconformability on any surface. Circuits were patterned on board of bilayer poly(lactic acid):PEDOT:PSS nanosheets[30] and similar nanosheets have been tested as ultrathin actuators and sensors.[31,32]

While all of the cited developments demonstrated the feasibility of realizing conformable electronic devices, their release, manipulation, and transfer still impose challenges, especially when the target surface is the skin or other biological tissues, such as the cerebral cortex of the brain. Rogers' group proposed the use of a silk fibroin layer used as bioresorbable (and edible) biointerface.[33] Alternatively, an elastomeric stamp or a water-soluble layer of poly(vinyl alcohol) is used for transfer.[34,35]

Nevertheless, current methods are rather unsatisfactory in terms of reliability and ease of release, manipulation and transfer, which are crucial from an end-user standpoint. A robust, low-cost, safe, and fully-integrated solution to these problems is required.

Wang's group used temporary transfer tattoo paper in the fabrication of a tattoo electrochemical sensor for physiological and security monitoring of chemicals,[36] and analytes in human sweat.[37–39] Energy harvesting from human perspiration with epidermal biofuel cells was also demonstrated.[5] These epidermal electrochemical devices are based on screen-printing of functional inks on temporary tattoo paper.[40]

In this paper, we report the use of decal transfer paper (temporary tattoo paper) as a novel unconventional substrate for the fabrication and release of ultraconformable conductive tattoo nanosheets with submicrometric thickness. To work on temporary transfer tattoo paper, we modified fabrication and patterning processes for obtaining freestanding conductive nanosheets that were recently reported by our group.[29,30,41] Thanks to this unconventional substrate, release and transfer of the tattoo nanosheet on the skin (or any other target surface) is easy, as in standard temporary tattoos for children: decal transfer paper is pressed against the skin and wet with water for a few seconds to permit release and adhesion of the tattoo. Moreover, we extended the capabilities of patterning on conductive nanosheets by the use of ink-jet materials printing. To this aim, we purposely chose a commercially available, high-conductivity PEDOT:PSS formulation in water that is specifically designed for ink-jetting. On the other hand, we found this formulation to be suitable for the spin-coating deposition

Dr. A. Zucca, Dr. Sudha, Dr. V. Mattoli, Dr. F. Greco
Center for Micro-BioRobotics @SSSA
Istituto Italiano di Tecnologia
Viale R. Piaggio 34, 56025 Pontedera, Italy
E-mail: virgilio.mattoli@iit.it; francesco.greco@iit.it
Dr. A. Zucca, Dr. C. Cipriani, S. Tarantino
The Biorobotics Institute
Scuola Superiore Sant'Anna
Viale R. Piaggio 34, 56025 Pontedera, Italy
Dr. Sudha, Dr. D. Ricci
Department of Robotics
Brain and Cognitive Science
Istituto Italiano di Tecnologia
Via Morego 30, 16163 Genova, Italy

DOI: 10.1002/adhm.201400761

ADVANCED HEALTHCARE MATERIALS
www.advhealthmat.de

Materials Views
www.MaterialsViews.com

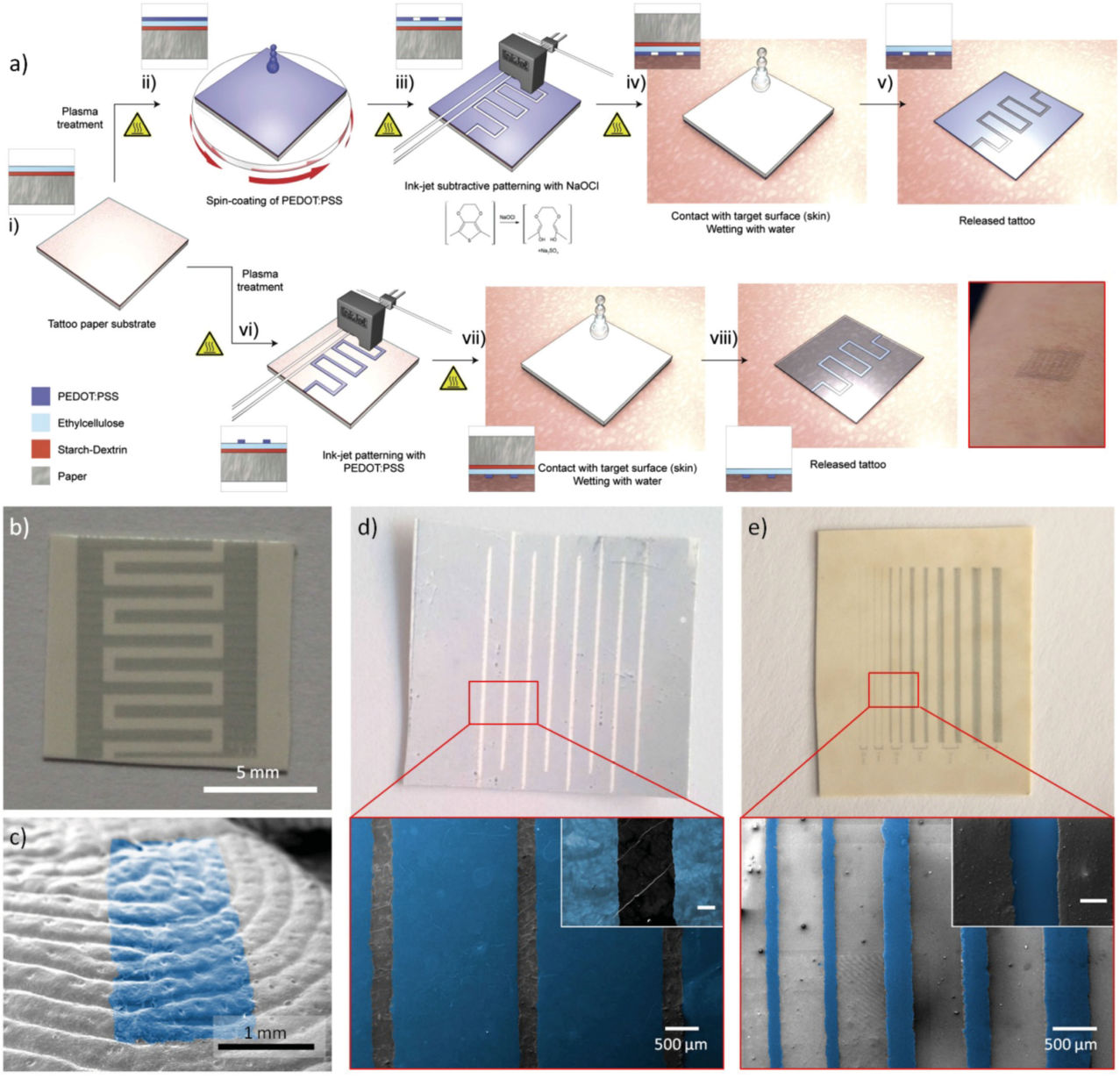

Figure 1. a) Scheme of bilayer ethylcellulose/PEDOT:PSS tattoo nanosheet fabrication, patterning and release/transfer on target surface (skin); b) tattoo nanosheet with interdigitated electrode pattern before release; c) colorized SEM image of tattoo nanosheet put in conformal contact to PDMS-replica of human skin. Patterned EC/PEDOT:PSS tattoo nanosheets: d) subtractive ink-jet patterning, line pattern with inter-electrode gap width 300 µm (inset: high-magnification image, scale bar 100 µm); e) additive patterning, printed lines with electrode width in the range 80–1000 µm (inset: high-magnification image, scale bar 50 µm). Conductive regions are highlighted in blue in colorized SEM images.

of homogeneous ultrathin nanofilms on tattoo decal transfer paper.

The overall process related to the fabrication, patterning, and release/transfer on target surface of tattoo nanosheets is schematically summarized in **Figure 1**a. The basic tattoo nanosheet is composed of an ethylcellulose (EC) layer and a PEDOT:PSS layer. It is noteworthy that the ultrathin EC layer is already contained in the decal transfer paper used as substrate and commercially available in a temporary tattoo paper kit. The decal transfer paper sheet consists of three layers: i) paper, ii) starch–dextrin coating (water-soluble layer), and iii) EC layer. Wetting the paper with water causes the release of a submicrometer thick EC film due to starch–dextrin dissolution. We investigated the properties of such EC film, finding interesting results in terms of its thickness and surface morphology as related to thermal behavior. These results are summarized in section S1.1 (Supporting Information). Various modifications of the process permitted to obtain bilayer EC/PEDOT:PSS as well as multilayer tattoo nanosheets. In one case, we purposely added a layer of poly(styrene) (PS) to the layers stack in order to provide an electrical insulating layer preventing the direct contact of the PEDOT:PSS with the target surface.

DOI: 10.1002/adhm.201400761

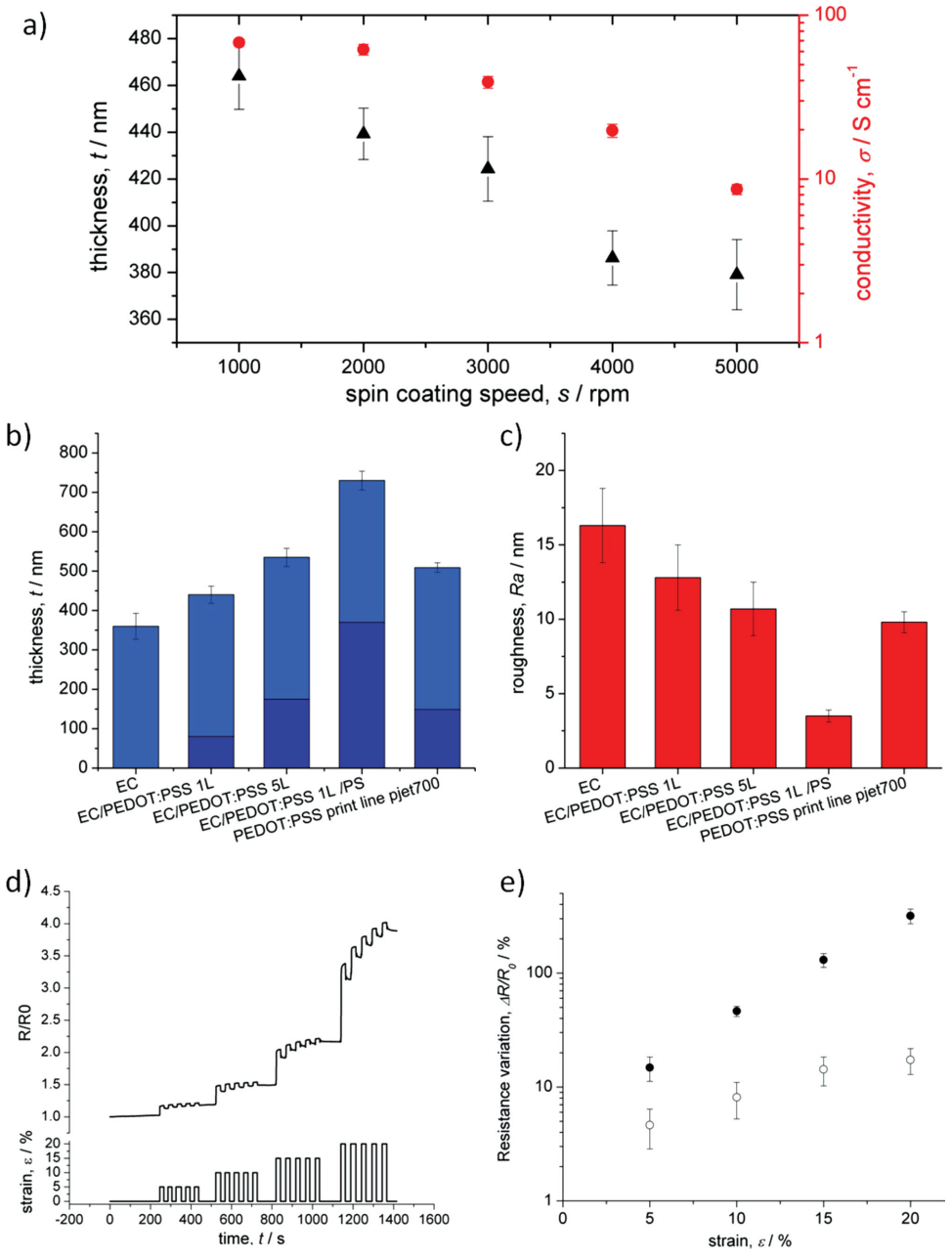

Figure 2. a) Thickness t and conductivity σ of EC/PEDOT:PSS nanosheet as a function of spin-coating speed s; comparison among nanosheets prepared with different processes and layer design: b) overall thickness t (EC thickness: cyan; PEDOT:PSS thickness: blue), c) average roughness R_a as obtained by AFM analysis on 10 μm × 10 μm images. Resistance variation of nanosheets during stretching test: d) normalized resistance variation R/R_0 (upper panel) versus time during repeated application of different strain values ε/% (lower panel) in a typical EC/PEDOT:PSS 1 L sample; e) average normalized resistance variation $\Delta R/R_0$ in stretching test on EC/PEDOT:PSS 1 L samples: irreversible (full circles) and reversible (open circles) contributions.

In **Figure 2**a, the thickness t of bilayer EC/PEDOT:PSS tattoo nanosheets is shown as a function of the speed s of a single PEDOT:PSS spin-coating deposition. The typical thickness of a tattoo nanosheet (i.e., the one obtained at s = 2000 rpm, selected for all further characterization and testing both for bilayer and multilayer nanosheets) was found to be t = 440 ± 22 nm, which includes an EC layer with an average thickness of 360 nm.

As the process and multilayer design were varied, the overall thickness of the tattoo nanosheet varied (Figure 2b). Five different tattoo nanosheet designs were compared, namely: 1) EC (EC single layer), 2) EC/PEDOT:PSS 1 L (bilayer with a single spin-coating of PEDOT:PSS on top of EC), 3) EC/PEDOT:PSS 5 L (5 times repeated spin-coating of PEDOT:PSS), 4) EC/PEDOT:PSS 1 L/PS (same design as in 2 + top insulating layer of PS), 5) EC/PEDOT:PSS print line (bilayer with ink-jet printed PEDOT:PSS).

The submicrometric thickness of tattoo nanosheets is crucial to attain ultra-conformability on complex surfaces as skin. Indeed, human epidermis is characterized by an extremely rich topography, made of a maze of ridges, furrows, and pores;[42] relief features found on human skin have typical lateral dimensions of 40–1000 μm and amplitude of 15–100 μm.[35] In the case of present tattoo nanosheets, their submicrometric thickness (tens of times less than typical height of skin relief microfeatures) is responsible for the decreased flexural rigidity: the tattoo can bend to extremely low bending radii and adapt to conformal contact on the skin microfeatures. Scanning electron microscope (SEM) image in Figure 1c shows a tattoo nanosheet put in conformal contact with a silicone replica of human skin.

Roughness of tattoo nanosheets was evaluated by means of atomic force microscope (AFM) image analysis, as this parameter affects conformability and stable interfacing. Differences in roughness of the EC surface with respect to PEDOT:PSS were evidenced (Figure 2c, and Figure S3a,b, Supporting Information), highlighting the well-known smoothing effect of PEDOT:PSS when spin coated on rough surfaces. A comparison of R_a as measured on nanosheets prepared with different processes and layer design was carried out (Figure 2c): as long as the number of PEDOT:PSS layers was increased (up to five layers, 5 L) a corresponding decrease in R_a was observed. An additional PS layer further smoothed down the nanosheet surface, as visible in AFM imaging (Figure S4, Supporting Information). Furthermore, the R_a of a printed line of PEDOT:PSS was comparable to that of a 5L bilayer (having a similar PEDOT:PSS thickness), unaffected by the roughness of the underlying EC.

An example of tattoo nanosheet release and transfer process is shown in the movie provided as Supporting Video 1 (Supporting Information). The tattoo nanosheets were released from the decal transfer paper sheet and transferred onto the desired target surface by wetting the paper with water as temporary tattoos for children.

In order to develop skin-contact electrodes and basic devices, the first challenge is to pattern the conductive layer of the tattoo to draw circuits. To this aim, two ink-jet patterning approaches were investigated: a subtractive and an additive technique. The advantage of using either mostly depends on the actual design of circuits and electrodes to be patterned. For example, subtractive technique is convenient in the case of electrodes with large area (i.e., several cm^2, which could be time-consuming to be ink-jet printed) separated by small insulating gaps. An example of interdigitated electrodes made using additive patterning is shown in Figure 1b. As concerns the subtractive technique, the patterning of the conductive PEDOT:PSS surface was provided by ink-jet printing of a sodium hypochlorite solution in water.[30] Such overoxidizing agent is known to cause an irreversible breaking of conjugation in polythiophenes, and consequently the loss of electrical conductivity.[43] Deactivation of the conductivity of the PEDOT:PSS was accompanied by concurrent change in color and degradation of the mechanical properties of the overoxidized film, which is eventually removed during the final washing step. The washing step was also necessary to remove any residual reactive salts. On the other hand, with an additive patterning technique, we directly provided an ink-jet printing deposition of the PEDOT:PSS solution on the EC layer.

The resolution and reproducibility of the two patterning techniques were evaluated by SEM imaging on lines printed in the range of width from 50 to 1000 μm. Minimum width of printed lines could be around 50 μm, for both additive and subtractive technique, because of the inherent spatial resolution of ink-jet printer that is limited to approximately 25 μm. Images in Figure 1d show an example of patterned EC /PEDOT:PSS 1L nanosheet (subtractive patterning technique), with an insulating line width of 300 μm. The blue portion of the colorized SEM image is the PEDOT:PSS (conductive) and the grayscale portion is the overoxidized/etched part (insulator). Conversely, Figure 1e shows an example of lines printed with an additive patterning technique (EC/PEDOT:PSS print line); the printed PEDOT:PSS line (colorized in blue in SEM image) has a width of 100 μm while the grayscale portion is the EC layer.

Conductivity σ of tattoo nanosheets with a single spin-coated PEDOT:PSS layer decreased with thickness (Figure 2a) as already reported for single-layer PEDOT:PSS nanofilms with similar range of thickness.[29] This behavior was rationalized by considering the variation of the effect of percolation arising at low thickness, comparable with the typical dimension of primary PEDOT-rich particles in PEDOT:PSS.[29,44] The typical conductivity of the tattoo nanosheets was in the range of 8–70 S cm^{-1}, as expected, given the PEDOT:PSS formulation used.

In order to investigate how mechanical stress affects nanosheet functionality, we measured the nanosheet electrical resistance during mechanical stimulation. We analyzed the resistance variation of tattoo nanosheets during repeated stretching by applying different degrees of strain with a dedicated setup (5%–10%–15%–20%). It was possible to distinguish two contributions to the overall resistance variation (Figure 2d). The first contribution was an irreversible change in resistance as the first stretch was applied, ascribable to the intrinsically limited stretchability of the PEDOT:PSS, as already observed by the group of Prof. Bao on PEDOT:PSS films deposited on stretchable poly(dimethylsiloxane) (PDMS) substrates.[28,45] Instead, during the following stretching cycles (at the same strain level), the nanosheet showed a reversible behavior (recovering completely the resistance variation induced by the strain). Furthermore, over 10% strain amount, an incomplete recovery of the resistance was observed also after the repeated stimulation; this effect, however, was less pronounced in repeated stimulation than during the first strain cycle. Variations of the resistance (reversible and irreversible contributions) as a function of the applied strain are summarized in Figure 2e.

The ability of the tattoo nanosheets to operate as conductors in conformal contact with target surfaces (i.e., paper, human skin) was demonstrated through some simple examples. In a first case, a tattoo nanosheet released on paper was used for turning on a LED (Figure S5a; video available as Supporting Video 1, Supporting Information). In a second example, we qualitatively tested tattoo nanosheet operation on human skin during exercise. A tattoo nanosheet was transferred on the skin and connected with two silver cotton wires for detecting the flexion/extension movements of the wrist through the resistance variation (Figure S5b, Supporting Information).

Thanks to their good conductivity, ultraconformability onto the skin also when dry, extreme lightweight, and ease of transfer, conductive tattoo nanosheets are envisioned as very

DOI: 10.1002/adhm.201400761

convenient and unperceivable human-device interfaces for physiological measurement on skin. In particular, they are especially suited for recording the electric activity of muscles: we tested the tattoo nanosheets as dry electrodes for surface electromyography (sEMG)

Such technique permits to evaluate and record the electrical activity produced by skeletal muscles. It is used as a diagnostic tool for identifying motor control disorders and various neuromuscular diseases or to analyze the biomechanics of movement in animals and humans.[46] State of the art sEMG electrodes comprise dry and gelled electrodes.[47] Dry electrodes, typically in the form of stiff metal pads (such as stainless steel), lack conformability and thus suffer from poor adhesion with the skin, which results in a high-impedance contact. Gelled electrodes refer to the most commonly used Ag/AgCl electrodes, which utilize an electrolytic gel to form a conductive path between skin and electrode, and nicely adhere to the skin due to their conformability. For chronic use, however, the reliance on an electrolyte leads to reduced signal quality as the gel dehydrates and the reapplication of gel may not be feasible. Hence gelled electrodes are typically used for acute recordings in research[48] or diagnostic applications (e.g., for heart beat monitoring). The advantages and disadvantages of dry and gelled electrodes were nicely resumed by Searle and Kirkup in their work.[47]

In this work, we used tattoo nanosheets as sEMG electrodes and we compared the recorded signals with those recorded by state of the art pregelled Ag/AgCl electrodes in pilot recordings. Surface EMGs were collected from the flexor carpi ulnaris muscles of one healthy subject, free of any neurological or motor disorders (**Figure 3**a). The spectrogram of the recordings and the normalized power spectral density (PSD) (Figure 3b,c) of the EMGs at different contraction levels were estimated using the fast Fourier transform in order to highlight differences between electrodes, within the spectrum of interest (<500 Hz). Although preliminary, the measurements match remarkably well at all contraction levels (Figure 3 and Figure S6, Supporting Information); this demonstrates that tattoo nanosheets can be used as bioelectrodes to pick-up the signal in the spectrum of the EMG. Detailed experimental methods and results are given in Supporting Information. As the voltage and spectrum ranges of the signals recorded during these tests is comparable to those typically found in electrocorticography (ECoG), we can also envisage to take advantage of the superior conformability, adhesion, and lightweight of the tattoo nanosheets for recording neural activity from large areas of the brain while faithfully following sulci and gyri of the cortex.

One of the most fascinating fields of use of EMG is prosthetic limbs.[49] Humans can contract skeletal muscles voluntarily, and in fact, the envelope of the EMG signal is broadly proportional to the level of contraction of the muscle being recorded. In addition, contractions related to different body movements can be recorded by multielectrode systems and recognized by suitable processing algorithms. As such EMGs can be used to control the movements of a prosthetic hand, arm, or leg. In this work, we proved that EMGs recorded from nanosheet tattoo electrodes can be used to control multiple movements of an artificial hand prosthesis. In particular, our system was able to recognize five different muscular patterns underlying five functional postures/grasps by recording EMG signal through four pairs of tattoo nanosheets placed on the forearm of one healthy subject, and to send the appropriate commands to a multigrasp robotic hand in real time (Figure 3d). The working system (classification accuracy > 90%) is demonstrated in the video provided as Supporting Video 2 (Supporting Information). As regards durability of the tattoo electrodes, continuous use of tattoos for as many as 8 h was involved during measurements. Electrodes worn for up to 12 h on the forearm showed no degradation, delamination, or irritation to the skin. Removal of tattoo electrodes from skin was easily obtained by washing (water and soap) or rubbing with a wet paper towel, as in the case of temporary transfer tattoos (Figure S5c, Supporting Information).

In conclusion, we demonstrated the fabrication of conductive nanosheets and their release and transfer as temporary transfer tattoos, which are characterized by ultraconformable adhesion and intimate integration with skin and other target surfaces.

The conducting tattoo nanosheets introduced here can represent a suitable platform for the development of soft, ultralightweight electrodes, sensing devices, and electronic systems with applications in healthcare, sport, and distributed sensing.

As a first demonstration of application in skin-contact sensing, tattoo nanosheets successfully performed as dry sEMG electrodes, showing comparable results with respect to bulky state of art EMG electrodes commonly used in clinical practice. Control of a robotic hand through EMG signals recorded with tattoo nanosheets on skin is also successfully demonstrated.

The ink-jet printing patterning method is suitable for further developing this platform toward more complex architectures and challenging applications, such as noninvasive multielectrode EMG and ECoG arrays on tattoo.

Experimental Section

Materials: Commercially available transfer tattoo base paper (Tattoo 2.1, The Magic Touch Ltd., UK) was purchased from Memo s.r.l. (Milan, Italy). A PEDOT:PSS aqueous dispersion, Clevios P Jet 700 (H.C. Starck GmbH, Leverkusen, Germany) has been employed after filtration (Minisart, average pore size 1.20 μm, Sartorius). Sodium hypochlorite solution (purum, ≈10%; Sigma–Aldrich), and the nonionic surfactant Triton X-100 (laboratory grade, Sigma–Aldrich) were used without any further purification. Polystyrene (PS, average M_w = 35 kDa) was purchased from Sigma–Aldrich and used as received. PDMS (Sylgard 184 silicone elastomer base and curing agent) was purchased from Dow Corning Corp .

Fabrication and Release of Conductive Tattoo Nanosheets: The overall process related to the fabrication, patterning, and release/transfer on target surface of tattoo nanosheets is summarized in Figure 1a, steps i–viii. i) The decal transfer paper sheet was cured at T = 180 °C for 20 min, cut in squares of 2.5 cm length, and blown with compressed air gun. Air plasma activation (15 s, 5 W, Colibri`plasma system, Gambetti, Italy) of the surface was performed in order to improve its wettability. ii) The PEDOT:PSS water dispersion was spin-coated at spin rate s = 2000 rpm for 60 s. For thicker PEDOT:PSS layers, the spin-coating process was repeated for multiple times, with an annealing at T = 120 °C and an air plasma treatment for 10 s at 5 W after each spin-coating step. Samples were also prepared by varying the spin rate from 1000 rpm to 5000 rpm to test the process and the conductivity of layers. Samples underwent a thermal treatment (30 minutes; T = 125 °C). The freestanding bilayer tattoo nanosheet was finally released from the transfer paper by dissolving the starch-dextrin sacrificial layer with DI water. Release and attachment on target surfaces was accomplished by placing the transfer

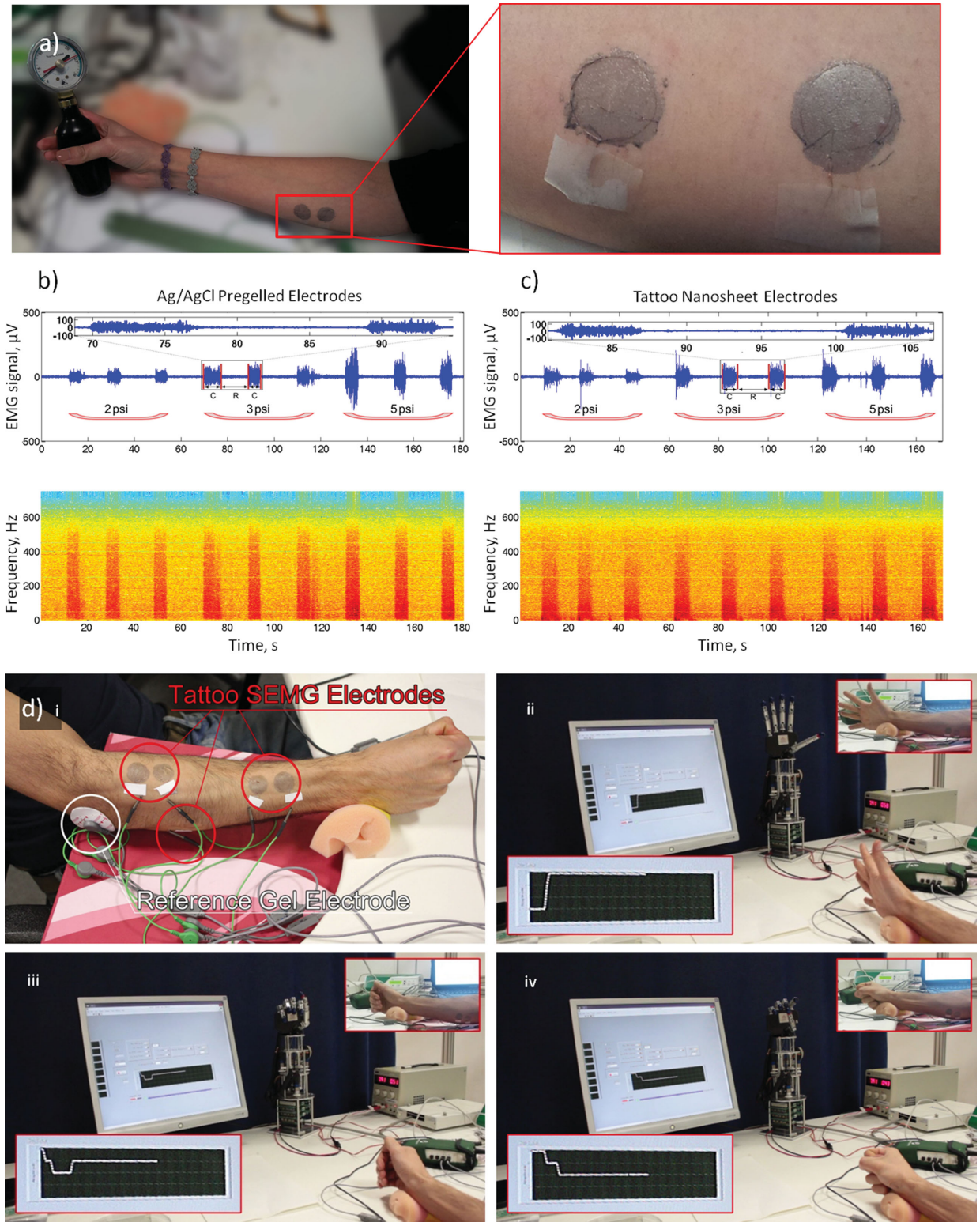

Figure 3. a) Tattoo nanosheets used as sEMG electrodes placed on the *flexor carpi ulnaris* muscle of one subject performing isometric contractions (subject grasped an analogue pressure gauge). Time domain and spectrograms of the EMG signals recorded during three series of grasping at different pressures (2, 3, 5 pounds/in.^{2}, psi) and rest; b) signal picked up by state of art Ag/AgCl pregelled electrodes and c) by tattoo nanosheet electrodes. d) Control of a robotic hand using tattoo nanosheet electrodes: i) Placement of the electrodes on the subject's forearm; ii–iv) examples of robot hand control in three different positions: ii) open (fully extended fingers); iii) lateral grip; iv) closed. A complete video is available in Supporting Video 2 (Supporting Information).

Adv. Healthcare Mater. **2015**,
DOI: 10.1002/adhm.201400761

in position on the target surface, wetting the paper with a wet cloth or water and pressing firmly for approximately 30 s, then sliding away transfer paper (steps iv–v or vii–viii in Figure 1a). Multilayer nanofilms EC/PEDOT:PSS 1L/PS were fabricated by adding one top layer of PS at a spin coating rate $s = 4000$ rpm for 40 s, followed by heating at $T = 80$ °C for 1 min on a hotplate.

Tattoo Nanosheet Patterning: Conductive patterns on tattoo nanosheets were obtained by including a step of ink-jet printing in the fabrication process by using a Dimatix Materials Printer DMP- 2800 (Fujifilm Corp., Japan). Subtractive patterning of the tattoo (localized overoxidation of PEDOT:PSS surface) was performed by ink-jet printing a NaClO solution (2 wt% + 0.13 wt% Triton X-100, in water), step iii in Figure 1a. A thermal treatment on a hot plate at $T = 50$ °C for 20 min was then operated on the sample, followed by rinsing the patterned surface with DI water and drying with nitrogen gun. Immersion in water and washing of back surface (paper) was strictly avoided for not permitting early dissolution of starch and release of nanosheet. Alternatively, additive patterning of tattoo nanosheets was accomplished by direct ink-jet printing of PEDOT:PSS on the EC layer, followed by a thermal treatment at $T = 125$ °C for 30 min, step vi in Figure 1a.

Structural, Electrical, and Mechanical Characterization: Thickness analysis was carried out with a P6 stylus profilometer (KLA Tencor-USA). All measurements were performed in air, at room temperature, re-collected on nanosheets, and dried on a clean Si wafer after release in water. The thickness t was measured by scratching the nanosheet with a needle and by measuring the height profile of the edge. Surface topography and roughness were investigated by AFM imaging, using a Veeco Innova scanning probe microscope operating in tapping mode, with silicon AFM Probes (NSG01, NT-MDT, Russia) at a resonant frequency of ≈150 kHz. The analysis of AFM images and calculation of the average roughness R_a were performed with the software Gwyddion SPM (available at http://gwyddion.net). Electrical resistance R and DC conductivity σ were measured with a two-point measurement on square samples with lateral dimension of 1.5 cm across metal electrodes with same width. Conductivity σ has been calculated by making use of formulae: $R = \rho\ (l/A)$; $\sigma = 1/\rho$ where ρ was the resistivity of the nanosheet and l and $A = lt$ were, respectively, the length and the cross-sectional area of the sample. The effects of mechanical stimulation on the electrical properties were investigated with a home-made platform and a dedicated software; tattoo nanosheets were re-collected on a PDMS slab and were linked to a slider and a load cell. The mechanical stimulus was applied with a micrometric slider; velocity and displacement were recorded by using a dedicated software developed in VisualStudio 2008 and a motor controller (c-863 Mercury servo motor controller, PI, USA). A load cell (LRF400, Futek, USA) opposite to the slider recorded the force required to induce a given deformation. Stretching tests were performed by imposing a complete strain cycle with duration of 20 s while the electrical impedance was simultaneously recorded by using two copper electrodes connected to an LCR meter (E4948A, Agilent Technologies, USA). All data have been recorded by using an acquisition system (NI USB-6218, National Instruments, USA).

sEMG Signals Recording and Control of Robotic Hand: Experiments of sEMG signals recording involving human subjects were carried on authors of the paper. Tattoo materials that came into direct contact with the skin are biocompatible. Continuous use of tattoos for as many as 8 h was involved during measurements. Electrodes worn for up to 12 h on the forearm showed no degradation or irritation to the skin. Two circular tattoo electrodes (diameter 20 mm) were placed above the *flexor carpi ulnaris* of the right forearm (interelectrode distance 25 mm) (Figure 3a), whereas two pregelled Ag/AgCl electrodes (Eurotrode PSG50S) with identical shape and size were placed symmetrically on the left forearm, in order to allow for comparison. The subject was asked to grasp an analogue pressure gauge (North Coast Medical, Morgan Hill, CA) and to maintain the grip force at three levels (2, 3, 5 pounds/in.^{2}, psi) as indicated by the gauge (Figure 3a), while the EMG was being recorded. Raw surface EMG data were collected using the Noraxon TeleMyo 2400R (Noraxon, Scottsdale, AZ, USA) through a wireless unit (TeleMyo 2400T). Raw data were hardware filtered (high pass: 10 Hz – first order; low pass: 500 Hz – eighth order; gain: 1000), acquired (sampling frequency: 1.5 kHz; resolution: 12 bits), and stored in a PC for an offline analysis. The signals were software filtered (six order 48–52 Hz, Butterworth stop band filter), divided in epochs of 1 s and the fast Fourier transform within the spectrum of interest (10–500 Hz) was computed for each epoch, in Matlab (MathWorks, Natick, MA). The robotic hand was controlled using an online EMG pattern recognition system available in our lab (akin the system described by Cipriani and co-workers).[50] Four pairs of electrodes were placed on the forearm of one healthy subject (Figure 3d) in order to gather signals from extrinsic flexor and extensor muscles of the hand. Signals were recorded using the Noraxon system (details above) band-pass filtered in hardware (high pass: 10 Hz–1st order; low pass: 1000 Hz–8th order; gain: 5000) and collected differentially at a sampling rate of 1.5 kHz by a data acquisition board on a Personal Computer running a custom LabView application. Data were windowed and for each window, time-domain features were extracted and fed into a Support Vector Machine (SVM) algorithm, which provided the classification output every 50 ms. As a result, every 50 ms a new command was sent from the PC to the hand via a serial connection and the hand moved accordingly. Signal processing, feature extraction, and validation are described in detail in the Supporting Information.

Supporting Information

Supporting Information is available from the Wiley Online Library or from the author.

Acknowledgements

This research was partly supported by the interdepartmental project "All polymer ultrathin conformable and stretchable large area epicortical electrode arrays", funded by the Istituto Italiano di Tecnologia.

Received: December 1, 2014
Revised: February 4, 2015
Published online:

[1] S. Bauer, *Nat. Mater.* **2013**, *12*, 871.
[2] M. L. Hammock, A. Chortos, B. C. K. Tee, J. B. H. Tok, Z. Bao, *Adv. Mater.* **2013**, *25*, 5997.
[3] H. Tao, M. A. Brenckle, M. Yang, J. Zhang, M. Liu, S. M. Siebert, R. D. Averitt, M. S. Mannoor, M. C. McAlpine, J. A. Rogers, D. L. Kaplan, F. G. Omenetto, *Adv. Mater.* **2012**, *24*, 1067.
[4] R. D. Kornbluh, R. Pelrine, H. Prahlad, A. Wong-Foy, B. McCoy, S. Kim, J. Eckerle, T. Low, *MRS Bull.* **2012**, *37*, 246.
[5] W. Jia, G. Valdés-Ramírez, A. J. Bandodkar, J. R. Windmiller, J. Wang, *Angew. Chem.* **2013**, *125*, 7374.
[6] S. Bauer, S. Bauer-Gogonea, I. Graz, M. Kaltenbrunner, C. Keplinger, R. Schwödiauer, *Adv. Mater.* **2014**, *26*, 149.
[7] T. Someya, *Stretchable Electron.* **2012**.
[8] D.-H. Kim, J. Xiao, J. Song, Y. Huang, J. A. Rogers, *Adv. Mater.* **2010**, *22*, 2108.
[9] T. Someya, Y. Kato, T. Sekitani, S. Iba, Y. Noguchi, Y. Murase, H. Kawaguchi, T. Sakurai, *Proc. Natl. Acad. Sci. U.S.A.* **2005**, *102*, 12321.
[10] A. Bonfiglio, D. De-Rossi, T. Kirstein, I. R. Locher, F. Mameli, R. Paradiso, G. Vozzi, *IEEE Trans. Information Technol. Biomed.* **2005**, *9*, 319.
[11] D.-H. Kim, N. Lu, R. Ma, Y.-S. Kim, R.-H. Kim, S. Wang, J. Wu, S. M. Won, H. Tao, A. Islam, K. J. Yu, T.-i. Kim, R. Chowdhury,

M. Ying, L. Xu, M. Li, H.-J. Chung, H. Keum, M. McCormick, P. Liu, Y.-W. Zhang, F. G. Omenetto, Y. Huang, T. Coleman, J. A. Rogers, *Science* **2011**, *333*, 838.
[12] M. Kaltenbrunner, T. Sekitani, J. Reeder, T. Yokota, K. Kuribara, T. Tokuhara, M. Drack, R. Schwödiauer, I. Graz, S. Bauer-Gogonea, S. Bauer, T. Someya, *Nature* **2013**, *499*, 458.
[13] J. Viventi, D.-H. Kim, L. Vigeland, E. S. Frechette, J. A. Blanco, Y.-S. Kim, A. E. Avrin, V. R. Tiruvadi, S.-W. Hwang, A. C. Vanleer, D. F. Wulsin, K. Davis, C. E. Gelber, L. Palmer, J. Van der Spiegel, J. Wu, J. Xiao, Y. Huang, D. Contreras, J. A. Rogers, B. Litt, *Nat. Neurosci.* **2011**, *14*, 1599.
[14] D.-H. Kim, J. Viventi, J. J. Amsden, J. Xiao, L. Vigeland, Y.-S. Kim, J. A. Blanco, B. Panilaitis, E. S. Frechette, D. Contreras, D. L. Kaplan, F. G. Omenetto, Y. Huang, K.-C. Hwang, M. R. Zakin, B. Litt, J. A. Rogers, *Nat. Mater.* **2010**, *9*, 511.
[15] D. Khodagholy, T. Doublet, M. Gurfinkel, P. Quilichini, E. Ismailova, P. Leleux, T. Herve, S. Sanaur, C. Bernard, G. G. Malliaras, *Adv. Mater.* **2011**, *23*, H268.
[16] P. Leleux, J.-M. Badier, J. Rivnay, C. Bénar, T. Hervé, P. Chauvel, G. G. Malliaras, *Adv. Healthcare Mater.* **2014**, *3*, 490.
[17] D. H. Kim, N. Lu, R. Ma, Y. S. Kim, R. H. Kim, S. Wang, J. Wu, S. M. Won, H. Tao, A. Islam, K. J. Yu, T. I. Kim, R. Chowdhury, M. Ying, L. Xu, M. Li, H. J. Chung, H. Keum, M. McCormick, P. Liu, Y. W. Zhang, F. G. Omenetto, Y. Huang, T. Coleman, J. A. Rogers, *Science* **2011**, *333*, 838.
[18] S. Wagner, S. Bauer, *MRS Bull.* **2012**, *37*, 207.
[19] Z. Suo, *MRS Bull.* **2012**, *37*, 218.
[20] J. A. Rogers, T. Someya, Y. Huang, *Science* **2010**, *327*, 1603.
[21] R. C. Webb, A. P. Bonifas, A. Behnaz, Y. Zhang, K. J. Yu, H. Cheng, M. Shi, Z. Bian, Z. Liu, Y.-S. Kim, W.-H. Yeo, J. S. Park, J. Song, Y. Li, Y. Huang, A. M. Gorbach, J. A. Rogers, *Nat. Mater.* **2013**, *12*, 938.
[22] H. Cheng, Y. Zhang, X. Huang, J. A. Rogers, Y. Huang, *Sens. Actuators A: Phys.* **2013**, *203*, 149.
[23] X. Huang, Y. Liu, H. Cheng, W.-J. Shin, J. A. Fan, Z. Liu, C.-J. Lu, G.-W. Kong, K. Chen, D. Patnaik, S.-H. Lee, S. Hage-Ali, Y. Huang, J. A. Rogers, *Adv. Funct. Mater.* **2014**, *24*, 3846.
[24] T. Sekitani, U. Zschieschang, H. Klauk, T. Someya, *Nat. Mater.* **2010**, *9*, 1015.
[25] T. Sekitani, S. Iba, Y. Kato, Y. Noguchi, T. Someya, T. Sakurai, *Appl. Phys. Lett.* **2005**, *87*, 1.
[26] M. Kaltenbrunner, M. S. White, E. D. Głowacki, T. Sekitani, T. Someya, N. S. Sariciftci, S. Bauer, *Nat. Commun.* **2012**, *3*, 770.
[27] D. J. Lipomi, B. C. K. Tee, M. Vosgueritchian, Z. Bao, *Adv. Mater.* **2011**, *23*, 1771.
[28] M. Vosgueritchian, D. J. Lipomi, Z. Bao, *Adv. Funct. Mater.* **2012**, *22*, 421.
[29] F. Greco, A. Zucca, S. Taccola, A. Menciassi, T. Fujie, H. Haniuda, S. Takeoka, P. Dario, V. Mattoli, *Soft Matter* **2011**, *7*, 10642.
[30] F. Greco, A. Zucca, S. Taccola, B. Mazzolai, V. Mattoli, *ACS Appl. Mater. Interfaces* **2013**, *5*, 9461.
[31] S. Taccola, F. Greco, B. Mazzolai, V. Mattoli, E. W. H. Jager, *J. Micromech. Microeng.* **2013**, *23*, 117004.
[32] S. Taccola, F. Greco, A. Zucca, C. Innocenti, C. De Julián Fernández, G. Campo, C. Sangregorio, B. Mazzolai, V. Mattoli, *ACS Appl. Mater. Interfaces* **2013**, *5*, 6324.
[33] D.-H. Kim, J. Viventi, J. J. Amsden, J. Xiao, L. Vigeland, Y.-S. Kim, J. A. Blanco, B. Panilaitis, E. S. Frechette, D. Contreras, D. L. Kaplan, F. G. Omenetto, Y. Huang, K.-C. Hwang, M. R. Zakin, B. Litt, J. A. Rogers, *Nat. Mater.* **2010**, *9*, 511.
[34] J.-W. Jeong, W.-H. Yeo, A. Akhtar, J. J. S. Norton, Y.-J. Kwack, S. Li, S.-Y. Jung, Y. Su, W. Lee, J. Xia, H. Cheng, Y. Huang, W.-S. Choi, T. Bretl, J. A. Rogers, *Adv. Mater.* **2013**, *25*, 6839.
[35] W.-H. Yeo, Y.-S. Kim, J. Lee, A. Ameen, L. Shi, M. Li, S. Wang, R. Ma, S. H. Jin, Z. Kang, Y. Huang, J. A. Rogers, *Adv. Mater.* **2013**, *25*, 2773.
[36] J. R. Windmiller, A. J. Bandodkar, G. Valdes-Ramirez, S. Parkhomovsky, A. G. Martinez, J. Wang, *Chem. Commun.* **2012**, *48*, 6794.
[37] A. J. Bandodkar, V. W. S. Hung, W. Jia, G. Valdes-Ramirez, J. R. Windmiller, A. G. Martinez, J. Ramirez, G. Chan, K. Kerman, J. Wang, *Analyst* **2013**, *138*, 123.
[38] A. J. Bandodkar, D. Molinnus, O. Mirza, T. Guinovart, J. R. Windmiller, G. Valdés-Ramírez, F. J. Andrade, M. J. Schöning, J. Wang, *Biosens. Bioelectron.* **2014**, *54*, 603.
[39] T. Guinovart, A. J. Bandodkar, J. R. Windmiller, F. J. Andrade, J. Wang, *Analyst* **2013**, *138*, 7031.
[40] J. R. Windmiller, J. Wang, *Electroanalysis* **2013**, *25*, 29.
[41] F. Greco, A. Zucca, S. Taccola, A. Menciassi, P. Dario, V. Mattoli, *MRS Online Proc. Library* **2012**, *1403*, 0.
[42] Y. Masuda, M. Oguri, T. Morinaga, T. Hirao, *Skin Res. Technol.* **2014**, *20*, 299.
[43] T. A. Skotheim, J. Reynolds, *Conjugated Polymers: Processing and Applications*, CRC Press, Boca Raton, USA **2007**.
[44] C. M. Stafford, C. Harrison, K. L. Beers, A. Karim, E. J. Amis, M. R. VanLandingham, H.-C. Kim, W. Volksen, R. D. Miller, E. E. Simonyi, *Nat. Mater.* **2004**, *3*, 545.
[45] D. J. Lipomi, J. A. Lee, M. Vosgueritchian, B. C. K. Tee, J. A. Bolander, Z. Bao, *Chem. Mater.* **2012**, *24*, 373.
[46] R. Merletti, P. A. Parker, *Electromyography: Physiology, Engineering, and Non-invasive Applications*, Vol. *11*, John Wiley & Sons, Hoboken, USA **2004**.
[47] A. Searle, L. Kirkup, *Physiol. Measurement* **2000**, *21*, 271.
[48] T. Pistohl, C. Cipriani, A. Jackson, K. Nazarpour, *Ann. Biomedical Eng.* **2013**, *41*, 2687.
[49] K. Nazarpour, C. Cipriani, D. Farina, T. Kuiken, *Neural Syst. Rehabil. Eng., IEEE Trans.* **2014**, *22*, 711.
[50] C. Cipriani, C. Antfolk, M. Controzzi, G. Lundborg, B. Rosen, M. C. Carrozza, F. Sebelius, *Neural Syst. Rehabil. Eng., IEEE Trans.* **2011**, *19*, 260.

Adv. Healthcare Mater. **2015**,
DOI: 10.1002/adhm.201400761